# Nanoplasmonic molecular ruler for nuclease activity and DNA footprinting

**Fanqing Frank Chen[1,§,*], Gang L. Liu[2,*], Yadong Yin[1,3,5], Daniele Gerion[1], Siri Kunchakarra[1], Bipasha Mukherjee[1], Stephen D. Jett[4], David G. Bear[4], A. Paul Alivisatos[1,3], Luke P. Lee[2]**

[1] Lawrence Berkeley National Laboratory, Berkeley, CA 94720

[2] Biomolecular Nanotechnology Center, Department of Bioengineering, University of California at Berkeley, Berkeley, CA 94720

[3] Department of Chemistry, University of California, Berkeley, CA 94720

[4] Department of Cell Biology and Physiology and the Cancer Research and Treatment Center, University of New Mexico Health Sciences Center, Albuquerque, NM 87131

[5]Current address:Department of Chemistry, University of California at Riverside, Riverside, CA 92521

[§]Correspondence should be addressed to:

Fanqing Frank Chen (f_chen@lbl.gov)
Life Sciences Division
Lawrence Berkeley National Laboratory
MS977R0225A, 1 Cyclotron Rd.
Berkeley, CA 94720

**Word count:**
Abstract: 147
Main Text: 1500
Methods: 752

**References: 30**

**Figures: 4**

## Abstract

We have constructed a nanoplasmonic molecular ruler, which can perform label-free and real-time monitoring of DNA length changes and perform DNA footprinting. The ruler was created by tethering double-stranded DNA to single Au nanoparticles. The scattering spectra of Au-DNA nanoconjugates showed red-shifted peak plasmon resonance wavelength dependent on DNA length, which can be measured with sub-nanometer axial resolution, averaging ~1.24 nm peak wavelength shift per DNA base pair. The spectra of individual Au-DNA nanoconjugates in the presence of nuclease showed a time-resolved dependence on the reaction dynamics, allowing quantitative, kinetic and real-time measurement of nuclease activity. The ruler was further developed into a new DNA footprinting platform. We showed the specific binding of a protein to DNA and the accurate mapping of its footprint. This work promises a very fast and convenient platform for mapping DNA-protein interactions, for nuclease activity monitoring, and for other DNA size-based methods.

---

Interactions between nucleic acids and proteins are essential to genetic information processing. The detection of size changes in nucleic acids is the key to mapping such interactions, and usually requires the synthesis of oligonucleotide substrates with fluorescent, electrochemical or radioactive labels[1-3], especially for nuclease-based methods. Yet, real-time detection within small volumes remains a challenge in the era of microarray and microfluidic devices.

Surface plasmon resonance (SPR) spectroscopy is an ultrasensitive optical method that measures the refractive index or dielectric constant of liquids or media in contact with the surface of metallic thin films. Conventional bulk-scale SPR can measure the refractive index of thin dielectrics, small analyte concentration, protein-protein interaction, and DNA hybridization[4, 5]. A platform that allows for plasmon resonance sensing on a single metallic nanoparticle at high speed has been developed, and various methods have been reported for immobilizing biomolecules on metallic nanoparticles[6-14]. The plasmon resonance wavelengths of the Au or Ag nanoparticles shift in response to changes in their immediate environment, and the wavelength change can be detected using scattering or absorption spectroscopy. Recently, methods have been developed to tether synthesized DNA to highly water-soluble Au nanoparticles[15-19]. We have also previously used single gold and silver nanoparticle dimer to demonstrate nanoplasmonic distance measurement[20].

In this paper, we designed a nanoplasmonic molecular ruler, with a 54-base pair double-stranded DNA (dsDNA) as the enzymatic substrate and calibration standard, and conjugated to 20 nm Au nanoparticle (Fig 1, 2). The dsDNA contained cleavage sites for the endonucleases HinDIII, XhoI, SalI, and KpnI at nucleotide positions 12, 24, 36, and 48. The surface density of dsDNA on Au nanoparticles was controlled by their concentration ratio during immobilization. A 100:1 DNA:Au ratio was found to

be the best compromise to preserve the natural extension of dsDNA (Fig. 2a), while allowing accessibility to the nuclease[21] (Fig. 2b-3). The surface modification of Au nanoparticles with dsDNA was confirmed by transmission electron microscopy (TEM) (Fig. 2a) and by electrophoresis (Fig. 2b-2).

The scattering images and spectra of individual nanoconjugates were acquired using a dark-field microscopy system with a true-color imaging camera and a spectrometer. Interestingly, Au-phosphine (Au-ph, Fig. 2c-2), which carries no DNA but phosphine surfactant, and Au-phosphine-DNA (Au-DNA, Fig. 2c-3) exhibit different colors in yellow and red, respectively. Attachment of DNA seems to red shift the peak plasmon resonance wavelength of the Au nanoparticle by 67 nm (Fig. 2c-4). In order to investigate whether the nanoplasmonic resonance frequency shift of the Au-DNA nanoconjugate can accurately reflect DNA size change, we artificially produced DNA size standards by endonuclease cleavage. About 10 nanoconjugates from each sample were examined spectroscopically in dark field and the statistics of the plasmon resonance wavelengths are shown in Fig. 3. The Au-DNA nanoconjugates provide a new means for studying the kinetics of the nuclease enzymatic reactions. Real time measurement of endonuclease activity and kinetics for one model endonuclease XhoI was demonstrated, and the average plasmon resonance wavelength drops after the XhoI endonuclease reactions due to the loss of 30 base pairs of dsDNA (Fig. 3a and 3b). EDTA-induced inhibition of XhoI reaction can also be visualized (Fig. 3b). The salt concentration change was negligible, since all components were pre-incubated with the same reaction buffer (Fig. 3b).

We then focused on the size effect of the attached DNA. Au-DNA nanoconjugates were reacted with KpnI, SalI, XhoI, and HinDIII, which led to the loss of the first 6, 18, 30, and 42 base pairs from the distal end of the full-length dsDNA,

respectively. Fig. 3c-1 shows the typical scattering spectra and plasmon resonance wavelengths of Au-DNA nanoconjugates after the 1 hour cleavage reactions. Fig. 3c-2 shows the plasmon resonance spectra of single Au nanoparticles tethered with 0, 12, 24, 36, 48, and 54 bps of dsDNA. The average wavelengths blue shifts were approximately 67 nm, 62 nm, 45 nm, 28 nm, 10 nm and 0 nm, respectively. The plasmon resonance shift of the nanoparticle corresponded to the change of the dielectric layer around the nanoparticle and is related to the length of the digested dsDNA. Using the Mie scattering calculation program for coated Au nanoparticles[22], the equivalent dielectric constant, or refractive index of the biopolymer shell (dsDNA+phosphine), was obtained (Supplemental Table S1, Fig. S2, and Fig. 3c-2). The relationship between the dsDNA length and the equivalent refractive index showed a good agreement with the quadratic *Langevin* model[23] (red fitted curve in Fig. 3c-2 and Supplemental data). An average wavelength shift of ~1.24 nm/bp was observed. Note the full length of the complete dsDNA (~20 nm) is much longer than the effective Forster transfer distance (<10 nm), thus the molecular ruler has longer detection range than Forster resonance energy transfer (FRET).

Based on the established correlation curve between the changes in the plasmon wavelength and in the DNA size (Fig. 3c), the DNA length in a nuclease reaction can be determined, which allows us to measure the footprint of DNA-binding proteins. Here we used the EcoRI(Q111) protein as a model DNA binding protein in exonuclease DNA footprinting. EcoRI(Q111) is a non-catalytic, cleavage-defective variant of the EcoRI protein with amino acid residue 111 mutated to Glutamine (Q). EcoRI(Q111) still maintains specific binding activity to the sequence of GAATTC on dsDNA, but doe not cleave DNA[24, 25]. We have previously used EcoRI(Q111) to block a transcription elongation complex[26]. As depicted in Fig. 4a, EcoRI(Q111) binds to

GAATTC DNA sequence on the Au-DNA nanoconjugates. Subsequently an exonuclease enzyme, BAL31 (100nM final concentration), is introduced to degrade the untethered dsDNA end without any specificity. BAL31 is an exonuclease that degrades both 3' and 5' termini of dsDNA[27]. Fig. 4 b and c show the scattering spectra of the digested Au-DNA nanoconjugate without and with the bound EcoRI(Q111), respectively. For the DNA unbound by EcoRI(Q111), when digested by BAL31, the plasmon resonance wavelength of the nanoconjugate blue-shifted ~52 nm in 20 minutes and stabilized afterwards (blue square in Fig. 4d); while for the DNA bound by the EcoRI(Q111), the plasmon resonance wavelength of the nanoconjugate shifted a maximum of 25 nm in ~10 minutes and stabilized afterwards (red circles in Fig. 4d). The corresponding base pair of the degraded dsDNA was calculated according to the fitted quadratic *Langevin* model (Supplement). The BAL31 exonuclease digested almost all (~90%) of the 54 bps of the dsDNA while it digested only ~25 bps with the EcoRI(Q111) blocking procession of BAL31 exonuclease. The stalling point of the exonuclease is around 25+/-3 bps from the distal end of the DNA, which is approximately 7 bps from the GAATTC site, and is in perfect agreement with previous measurement results using conventional radiolabels (7+/-3 bps)[25]. Previous mapping indicates that EcoRI(Q111) binds to 3 bp of dsDNA flanking the 3' boundary of the GAATTC sequence, and the steric exclusion between EcoRI(Q111) and exonuclease contributes to the other 4 bps. A control exonuclease Exo-1, which does not cleave dsDNA, showed no effect on the ruler spectra (Fig. 4d).

The magnitudes of plasmon resonance shifts in our experiments are greater than those reported previously in other biochemical reactions such as protein binding. We attribute the relatively larger wavelength shift to the stiffness of dsDNA axially and the unique dependence of its dielectric constant on its length. Additionally, since the

proteins and DNA have distinct electron densities, there is a large difference in their scattering potential. It seems that the DNA scattering potential is one order of magnitude higher than proteins. Hence, the partial shortening or extension of the dsDNA will lead to a proportionally larger change around the Au surface compared to the change induced by a coiled protein binding or disassociation event. Furthermore, the reduction in the length of the dsDNA is also accompanied by a considerable decrease of its refractive index (Supplemental data, Table S1). An independent study by Doron-Mor et al showed coordination-based self-assembled multilayers can offer thickness tuning of Au nanoparticle SPR spectra in the range from 1-15nm[28, 29], further validating our observation of plasmonic spectra shift can be correlated with the length of the DNA. The irregularity in the size and shape of the Au nanoparticles is possibly a contributing factor in the broadening of the spectra, and the resulting standard deviation. The accuracy and spectral resolution of our measurements can be further improved by using nanoparticles with better shape and size control.

The time resolution of the nanoplasmonic biomolecular ruler can be as high as 1 spectrum per second by taking the advantage of the high quantum efficiency of Rayleigh scattering compared to fluorescence or Raman scattering; therefore the biomolecular reaction in the time scale of seconds can also be measured using our system. Even though only simple dsDNA substrate is used here, there is no limitation to either the sequences, or structure of the oligonucleotide substrates. The ability to resolve a single nanoparticle without the need for radioactive or fluorescent labeling also makes it possible to perform high-throughput screening in a high density microarray or microfluidic devices. The technology can also be used for the detection of other enzymes that induce length changes.

## Methods

### Preparation of the dsDNA-conjugated Au nanoparticle

The dsDNA (Fig. 1b and Supplement) was mixed with the concentrated phosphine-coated Au nanoparticles (Fig. 2b-1 and Supplement) in a molar ratio of 200:1, 100:1, 50:1, and 20:1, at room temperature for about 12 hours, then stored in -20 °C. Electrophoresis was used to verify the DNA attachment (Fig. 2b-2). The decreased mobility of the DNA-conjugated gold particles was clearly observed, indicating the successful DNA attachment to the gold nanoparticles. The presence of DNA can be confirmed by TEM imaging, with or without the Uranyl Acetate staining (provided by Mark Le Gros), while the extra stain further increased the effective diameter of the whole complex (Fig. 2a).

### Scattering imaging and spectroscopy of single Au-DNA nanoconjugates

The microscopy system consisted of a Carl Zeiss Axiovert 200 inverted microscope (Carl Zeiss, Germany) equipped with a darkfield condenser ($1.2 < NA < 1.4$), a true-color digital camera (CoolSNAP *cf*, Roper Scientific, NJ), and a 300 mm focal-length and 300 grooves/mm monochromator (Acton Research, MA) with a 1024 × 256-pixel cooled spectrograph CCD camera (Roper Scientific, NJ). A 2 $\mu$m-wide aperture was placed in front of the entrance slit of the monochromator to keep only a single nanoparticle in the region of interest. After photobleaching the fluorescence, the true-color scattering images of Au-DNA nanoconjugates were taken using a 60X objective lens (NA = 0.8) and the true-color camera with a white light illumination from a 100 W halogen lamp. The scattering spectra of Au-DNA nanoconjugates were routed to the monochromator and spectrograph CCD. Raw spectra were normalized

with respect to the spectrum of a non-resonant nanoparticle (*i.e.*, polystyrene) after the background subtraction. In the real-time spectroscopy experiments, the nanoparticle-immobilized glass slide was mounted on a transparent ITO heater with an external thermostat and heated to 37°C or 25°C. The immobilized nanoparticles were immersed in a drop of buffer solution which also served as the contact fluid for the dark-field condenser. The endonuclease or exonuclease enzymes with buffer solution were loaded by pipette into the contact fluid and the continuous spectrum acquisition started simultaneously. The microscopy system was completely covered by a dark shield, which prevents ambient light interference and excessive evaporation.

**Cleavage reaction of dsDNA on Au-DNA nanoparticle conjugate**

We immobilized the Au-DNA nanoconjugates electrostatically on an ultra-clean thin glass slide. Cleavage reaction for DNA was performed with endonucleases HinDIII, KpnI, XhoI, and SalI (Figure 2b-3), and 1 $\mu$L of the Au-DNA particle in a 100 $\mu$L final volume (3.5 nM final concentration for restriction enzymes), same as described in the Supplement S1, with the only modification of removing the reducing reagent from the reaction buffer and the enzymes, in order to avoid detachment of the thiolated DNA from the gold nanoparticle.

**Real time measurement of endonuclease activity, kinetics, and inhibition**

For kinetic measurement, XhoI is used as model enzyme. The cleavage was confirmed by FITC fluorescence images as well (Fig. 3a, panel 5, 6, and 7). The purpose of the FITC label removal experiment was solely for the validation of the enzymatic cleavage. The fluorescent label had no influence on the plasmon resonance measurement. The scattering spectra of the nanoconjugates were measured after the

fluorescence was photobleached. For real-time kinetics measurement, 1 spectrum with 10 second integration time was acquired for every minute. Significant blue shifts of the plasmon resonance wavelength were observed for the first 10 minutes and correlated with intensity decrease (Fig. 3b).

The rate of the endonuclease reaction on the Au-DNA nanoconjugate showed a concentration dependence, and was determined to followed a Michaelis-Menton enzyme kinetics[30] (Fig. 3). The inhibition of the endonuclease reactions on Au-DNA nanoconjugates were achieved with the simultaneous addition of 10 mM EDTA and the 3.5 nM XhoI enzymes, the $Mg^{2+}$ in the reaction buffer, which is required for XhoI activity, can be chelated by EDTA.

**BAL-31 reaction of EcoRI(Q111)-bound dsDNA-Au**

The cleavage-defective EcoRI(Q111) was purified according to previous description[24-26], and incubated at 100 nM final concentration with the immobilized Au-DNA nanoconjugates (with 5' thiolated oligo AAAGGATCCAAGCTT***GAATTC***-CTCGAGAGATCTGTCGACGATATCGGTACCAAA and its complementary strand, note FITC moiety was not synthesized for this dsDNA version, so that exonuclease cleavage would not be affected, while the thiolation scheme was kept) for 10 minutes in the 80 $\mu$L reaction buffer at 37°C. Afterwards, 20 $\mu$L BAL31 enzymes (Clontech, CA) was added into the reaction buffer containing immobilized Au-DNA nanoconjugates in a 100 $\mu$L final volume, with a BAL31 final concentration of 100nM. The binding buffer contains 50mM NaCl, 10mM $MgCl_2$, 0.025% Triton X-100, and 100mM Tris-HCl pH7.5 at 25°C.

**Acknowledgements**

This work was supported by DARPA, NIH grant R21CA95393 (F.F.C.), UCSF Prostate Cancer Grant (F.F.C.). This work was performed under the auspices of the U.S. Dept. of Energy, at the University of California/Lawrence Berkeley National Laboratory under contract no. DE-AC03-76SF00098.

**Supporting Information Available**

**References:**

1. Behrens, S., Fuchs, B.M. & Amann, R. The effect of nucleobase-specific fluorescence quenching on in situ hybridization with rRNA-targeted oligonucleotide probes. *Syst Appl Microbiol* **27**, 565-572 (2004).
2. Smith, J. & Anslyn, E.V. Radioactive End Labeling to Determine Hydrolytic Rates of Nuclease Mimics. *Anal Biochem* **220**, 53-57 (1994).
3. Hillier, S.C. et al. An electrochemical study of enzymatic oligonucleotide digestion. *Bioelectrochemistry* **63**, 307-310 (2004).
4. Homola, J., Yee, S.S. & Gauglitz, G. Surface plasmon resonance sensors: review. *Sensor Actuat B-Chem* **54**, 3-15 (1999).
5. Karlsson, R. SPR for molecular interaction analysis: a review of emerging application areas. *J Mol Recognit* **17**, 151-161 (2004).
6. Mulvaney, P. Surface plasmon spectroscopy of nanosized metal particles. *Langmuir* **12**, 788-800 (1996).
7. Elghanian, R., Storhoff, J.J., Mucic, R.C., Letsinger, R.L. & Mirkin, C.A. Selective colorimetric detection of polynucleotides based on the distance-dependent optical properties of gold nanoparticles. *Science* **277**, 1078-1081 (1997).
8. Eck, D., Helm, C.A., Wagner, N.J. & Vaynberg, K.A. Plasmon resonance measurements of the adsorption and adsorption kinetics of a biopolymer onto gold nanocolloids. *Langmuir* **17**, 957-960 (2001).
9. Englebienne, P., Van Hoonacker, A. & Verhas, M. High-throughput screening using the surface plasmon resonance effect of colloidal gold nanoparticles. *Analyst* **126**, 1645-1651 (2001).
10. Nath, N. & Chilkoti, A. A colorimetric gold nanoparticle sensor to interrogate biomolecular interactions in real time on a surface. *Anal Chem* **74**, 504-509 (2002).
11. Sun, Y.G. & Xia, Y.N. Increased sensitivity of surface plasmon resonance of gold nanoshells compared to that of gold solid colloids in response to environmental changes. *Anal Chem* **74**, 5297-5305 (2002).
12. McFarland, A.D. & Van Duyne, R.P. Single silver nanoparticles as real-time optical sensors with zeptomole sensitivity. *Nano Lett* **3**, 1057-1062 (2003).

13. Raschke, G. et al. Biomolecular recognition based on single gold nanoparticle light scattering. *Nano Lett* **3**, 935-938 (2003).
14. Oldenburg, S.J., Genick, C.C., Clark, K.A. & Schultz, D.A. Base pair mismatch recognition using plasmon resonant particle labels. *Anal Biochem* **309**, 109-116 (2002).
15. Alivisatos, A.P. et al. Organization of 'nanocrystal molecules' using DNA. *Nature* **382**, 609-611 (1996).
16. Zanchet, D., Micheel, C.M., Parak, W.J., Gerion, D. & Alivisatos, A.P. Electrophoretic isolation of discrete Au nanocrystal/DNA conjugates. *Nano Lett* **1**, 32-35 (2001).
17. Taton, T.A., Mirkin, C.A. & Letsinger, R.L. Scanometric DNA array detection with nanoparticle probes. *Science* **289**, 1757-1760 (2000).
18. Storhoff, J.J., Elghanian, R., Mucic, R.C., Mirkin, C.A. & Letsinger, R.L. One-pot colorimetric differentiation of polynucleotides with single base imperfections using gold nanoparticle probes. *J Am Chem Soc* **120**, 1959-1964 (1998).
19. Mirkin, C.A., Letsinger, R.L., Mucic, R.C. & Storhoff, J.J. A DNA-based method for rationally assembling nanoparticles into macroscopic materials. *Nature* **382**, 607-609 (1996).
20. Sonnichsen, C., Reinhard, B.M., Liphardt, J. & Alivisatos, A.P. A molecular ruler based on plasmon coupling of single gold and silver nanoparticles. *Nat Biotechnol* **23**, 741-745 (2005).
21. Parak, W.J. et al. Conformation of oligonucleotides attached to gold nanocrystals probed by gel electrophoresis. *Nano Lett* **3**, 33-36 (2003).
22. Bohren, C.F., Huffman, D. R. Absorption and Scattering of Light by Small Particles. (John Wiley & Sons, Inc., New York; 1983).
23. Mazur, J. & Jernigan, R.L. Distance-Dependent Dielectric-Constants and Their Application to Double-Helical DNA. *Biopolymers* **31**, 1615-1629 (1991).
24. King, K., Benkovic, S.J. & Modrich, P. Glu-111 Is Required for Activation of the DNA Cleavage Center of EcoRI Endonuclease. *J Biol Chem* **264**, 11807-11815 (1989).
25. Pavco, P.A. & Steege, D.A. Elongation by Escherichia coli RNA polymerase is blocked in vitro by a site-specific DNA binding protein. *J Biol Chem* **265**, 9960-9969 (1990).
26. Jett, S.D. & Bear, D.G. Snapshot Blotting - Transfer of Nucleic-Acids and Nucleoprotein Complexes from Electrophoresis Gels to Grids for Electron-Microscopy. *P Natl Acad Sci USA* **91**, 6870-6874 (1994).
27. Legerski, R.J., Hodnett, J.L. & Gray, H.B., Jr. Extracellular nucleases of pseudomonas BAL 31. III. Use of the double-strand deoxyriboexonuclease activity as the basis of a convenient method for the mapping of fragments of DNA produced by cleavage with restriction enzymes. *Nucleic Acids Res* **5**, 1445-1464 (1978).
28. Doron-Mor, I. et al. Sensitivity of transmission surface plasmon resonance (T-SPR) spectroscopy: Self-assembled multilayers on evaporated gold island films. *Chem-Eur J* **11**, 5555-5562 (2005).
29. Wanunu, M. et al. Branched coordination multilayers on gold. *J Am Chem Soc* **127**, 17877-17887 (2005).

30. Mizu, M., Koumoto, K., Kimura, T., Sakurai, K. & Shinkai, S. Protection of polynucleotides against nuclease-mediated hydrolysis by complexation with schizophyllan. *Biomaterials* **25**, 3109-3116 (2004).

**Figure legends**

**Figure 1. Design of the Au-DNA nanoplasmonic molecular ruler. (a)** Synthesis process of the single Au-DNA nanoconjugate. The 20 nm Au nanoparticle modified with a phosphine surfactant monolayer was enclosed by a layer of synthesized 54-bp dsDNA. A thiol group and FITC fluorophore were synthesized at each end of the dsDNA respectively. Through the thiol-Au chemistry, the dsDNA was tethered onto 20 nm Au nanoparticles. The dsDNA can be cleaved by 4 endonuclease enzymes, KpnI, SalI, XhoI, and HinDIII, with different incision lengths. **(b)** Sequence of the dsDNA. The incision sites of the enzymes are denoted on the respect positions of the dsDNA. The dsDNA contains restriction sites for the endonucleases HinDIII, XhoI, SalI, and KpnI, with their central incision positions at 12, 24, 36, and 48 bps from the Au nanoparticle-tethered end, respectively. The fluorescent labeling (FITC) is only for further confirmation of nuclease reactions, and thus not necessary for plasmon resonance measurements. The cleavage of the synthesized dsDNA with the endonucleases was confirmed by gel electrophoresis (Supplement Fig. S1).

**Figure 2. Properties of the nanoconjugates. (a)** TEM images of nanoconjugates. Shown are: (1) 20 nm Au nanoparticles, (2) Au-DNA nanoconjugates without fixation and staining, and (3) Au-DNA nanoconjugates (DNA:Au = 100:1 molar ratio) fixed and stained by Uranyl Acetate; (4) The gap distances between the Au nanoparticles in the three TEM images. The presence of DNA can be confirmed by the Uranyl Acetate staining, while the extra stain further increased the effective diameter of the whole complex. Uneven DNA density around the surface in Fig. 2a-2 is due to fixation and surface variations. **(b)** Gel electrophoresis of nanoconjugates. Shown are: (1) Au-

phosphine (Au-ph) nanoconjugates in different phosphine/Au ratios. The Au nanoparticles were stabilized through surface exchange with Bis(*p-sulfonatophenyl)phenylphosphine* (phosphine) to prevent aggregations. (2) Au-DNA nanoconjugates in different dsDNA/Au-ph ratios, and (3) Au-DNA nanoconjugates cleaved by 4 endonuclease enzymes, KpnI, SalI, XhoI, and HinDIII, with incisions that will lead to the loss of the first 6, 18, 30, and 42 base pairs from the distal end of the full-length dsDNA, respectively. The shorter the DNA, the faster the gel mobility is. **(c)** Darkfield scattering images of nanoconjugates. Shown are: (1) A single nanoparticle being targeted and isolated from a field of Au-DNA nanoparticles readily available for spectroscopic examination. The scattering image of a single nanoconjugate can be obtained on a B/W spectrograph CCD camera; shown here are the true-color scattering images of (2) Au-ph and (3) Au-DNA nanoconjugates. The nanoconjugate shown in panel 1 was selected for spectral examination by a 2 $\mu$m entrance slit (vertical) in front of the detector and by defining a region-of-interest (green, horizontal bars) in the software; (4) scattering spectra of the Au-ph and Au-DNA nanoconjugates. Au-DNA is red-shifted from 540 nm to 607 nm compared to Au-ph. Au-ph is the Au nanoparticle without DNA attachment and is the negative control here.

**Figure 3. Plasmon resonance shift detection of endonuclease enzymes with Au-DNA nanoconjugates. (a)** Plasmon resonance sensing with multiple nanoconjugates. Shown are: the darkfield scattering images of Au-DNA nanoconjugates (1) before, (2) 1 hr and (3)16 hr after the cleavage reaction by enzyme XhoI; (4) the plasmon resonance wavelengths of the single Au nanoconjugates in the three cases above. Also shown are: fluorescence images of Au-DNA nanoconjugates (5) before, (6) 1hr and (7) 16 hr after the cleavage reaction by enzyme XhoI. The fluorescence intensities at 4

different areas (red squares) in each case were measured and the statistics of the fluorescence intensities are shown in (8) with the average fluorescence intensity of the single Au nanoconjugates in the above three cases. Note the full length of the complete dsDNA (~20 nm) is much longer than the effective Forster transfer distance (<10 nm), and thus the FITC fluorophore at distal end of DNA was not quenched. The FITC fluorophore was detached from the Au nanoparticles and diffused into the buffer solution after the DNA cleavage, so that the overall fluorescence intensity at the image plane (where the Au nanoparticles are) decreased dramatically. **(b)** Real-time plasmon resonance sensing of endonuclease reactions by single Au-DNA nanoconjugate, with the peak plasmon resonance wavelength shown as a function of time. The Au-DNA nanoconjugates were illuminated with a white light source for 20 minutes to completely photobleach the fluorescence prior to the spectroscopic measurement. The continuous acquisition of the scattering spectrum of a selected nanoparticle starts in synchronization with the introduction of the XhoI enzymes with the final concentration of ~3.5 nM. One spectrum was taken every minute with a 10-second integration time. Shown are: (1) raw scattering spectra data of a single Au-DNA nanoconjugate in the first 10 minutes of endonuclease reaction; time-resolved. In the first 3 minutes, there were a temporary red shift of the plasmon resonance wavelength, an increase of scattering intensity, and a flattening of the spectra. The brief oscillation is likely due to the initial loading of the enzyme molecules onto the dsDNA before incision. (2) plasmon resonance peak wavelength and (3) scattering peak intensity of the Au-DNA nanoconjugate in the 30min reactions with 1:1 XhoI (3.5 nM final concentration, red circle), 1:10 XhoI (350 *p*M final concentration, orange triangle), control buffer solution only (blue diamond), and inhibitor/chelator EDTA (green square). The plasmon resonance wavelength data exhibits a first-order exponential decay (red and orange

curves). The rate of the endonuclease reaction on the Au-DNA nanoconjugate showed concentration dependence, and followed a Michaelis-Menton enzyme kinetics. The plasmon resonance wavelength of the nanoconjugate decreased at a slower rate with lower concentrations of enzymes. The reaction rate constants for these two concentrations of enzyme were $5.8 \times 10^{-3}$ $s^{-1}$ and $1.5 \times 10^{-3}$ $s^{-1}$, respectively. **(c)** Calibration curve generated by plasmon resonance sensing of multiple enzymes. Shown are (1) typical scattering spectra and (2) plasmon resonance peak wavelengths of the Au-DNA nanoconjugates after the cleavage reactions with 4 enzymes respectively, and as a function of the number of base pairs remain attached to the Au nanoparticle after the cleavage. We also estimated the equivalent refractive indices of the dsDNA after cleavages. The red curve is a fit from a semi-empirical model using a *Langevin*-type dependence of the refractive index vs. dsDNA length (Supplement).

**Figure 4. DNA footprinting of exonuclease stalled by the EcoRI(Q111) proteins.** (a) Schematic diagram of footprinting by BAL31 and the stalled BAL31 hydrolysis by DNA bound EcoRI(Q111) protein. The EcoRI(Q111) binds to GAATTC site on the DNA plus additional 3 bps on both flanks of GAATTC, and blocks nucleotide removal by BAL31 on a single Au-DNA nanoconjugate. The dsDNA is removed almost completely by the BAL31 enzyme in the absence of the EcoRI(Q111). However, after binding with EcoRI(Q111), the BAL31 exonuclease hydrolysis is stalled at 7+/-3 bp from the 3' end of GAATTC binding sequence due to the EcoRI(Q111) blockade. (b) Time-lapse scattering spectra of the single Au-DNA nanoconjugate without EcoRI(Q111) during the exonuclease BAL31 hydrolysis. (c) Time-lapse scattering spectra of the single Au-DNA nanoconjugate with EcoRI(Q111) during the exonuclease BAL31 hydrolysis. The plasmon resonance wavelength of a single

nanoconjugate in each of these two samples is monitored throughout the hydrolysis reactions in 21 minutes. (d) Plasmon resonance wavelength of the Au-DNA nanoconjugate as the function of time in the exonuclease reactions, with wavelength shift shown on right Y axis. Also shown on the left y axis is the digested base pair of the dsDNA as the function of time in the exonuclease reactions. The BAL31 maps the distal boundary of the DNA footprint to ~25 bp from the distal end of the DNA, which matches the previous measurement by radioactive footprinting method[25]. Previous mapping indicates that EcoRI(Q111) binds to 3 bp of dsDNA flanking the 3' boundary of the GAATTC sequence, and the steric exclusion between EcoRI(Q111) and the footprinting exonuclease contributes to the other 4 bps[25]. A control exonuclease Exo-1, which does not cleave dsDNA, is used as negative control here.

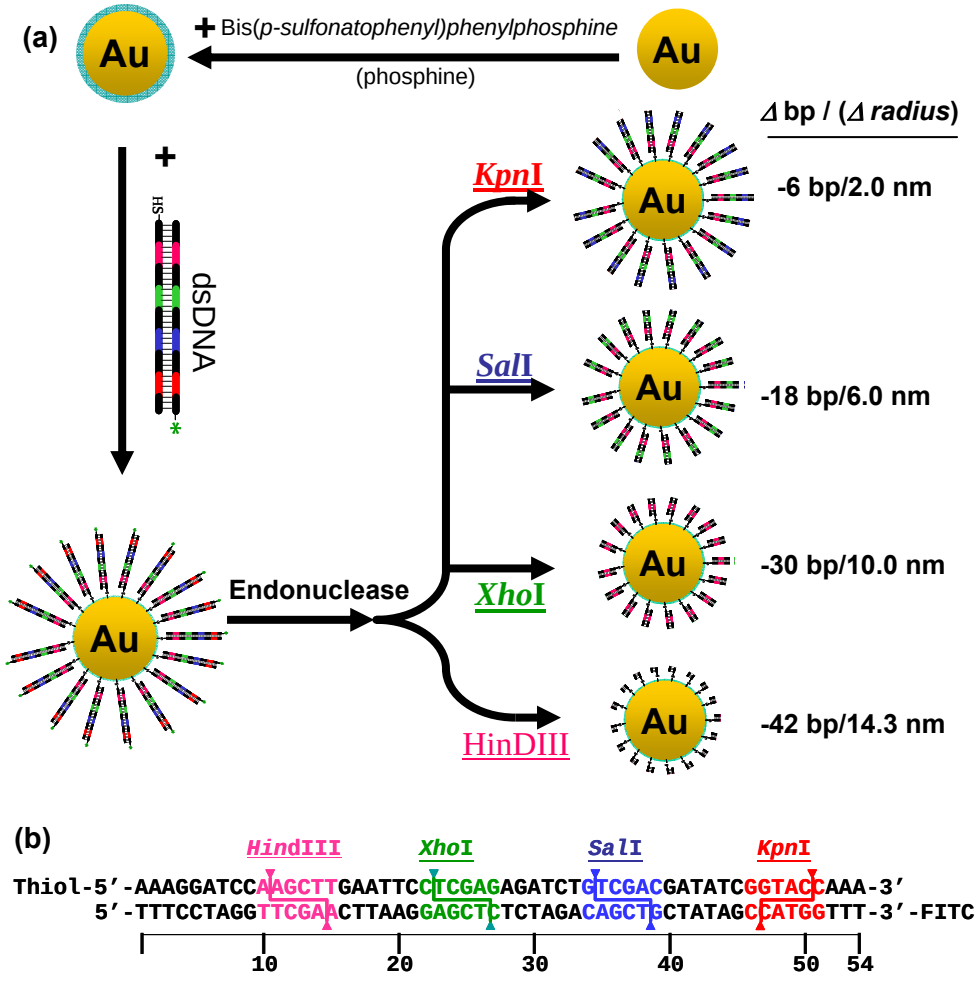
(a)
Au
+ Bis(p-sulfonatophenyl)phenylphosphine
(phosphine)
Au
Δ bp / (Δ radius)
+
HS-
dsDNA
*
KpnI
Au
-6 bp/2.0 nm
SalI
Au
-18 bp/6.0 nm
Au
Endonuclease
XhoI
Au
-30 bp/10.0 nm
HinDIII
Au
-42 bp/14.3 nm
(b)
HindIII
XhoI
SalI
KpnI
Thiol-5'-AAAGGATCCAAGCTTGAATTCCTCGAGAGATCTGTCGACGATATCGGTACCAAA-3'
5'-TTTCCTAGGTTCGAACTTAAGGAGCTCTCTAGACAGCTGCTATAGCCATGGTTT-3'-FITC
10
20
30
40
50
54

Figure 1

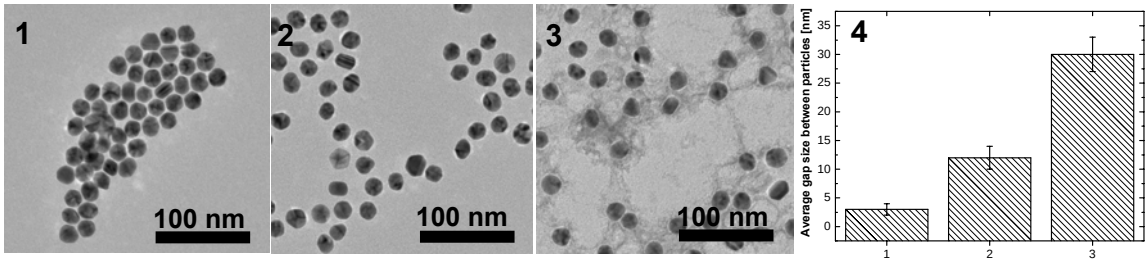
1
100 nm
2
100 nm
3
100 nm
4
Average gap size between particles [nm]
0
5
10
15
20
25
30
35
1
2
3

(a)

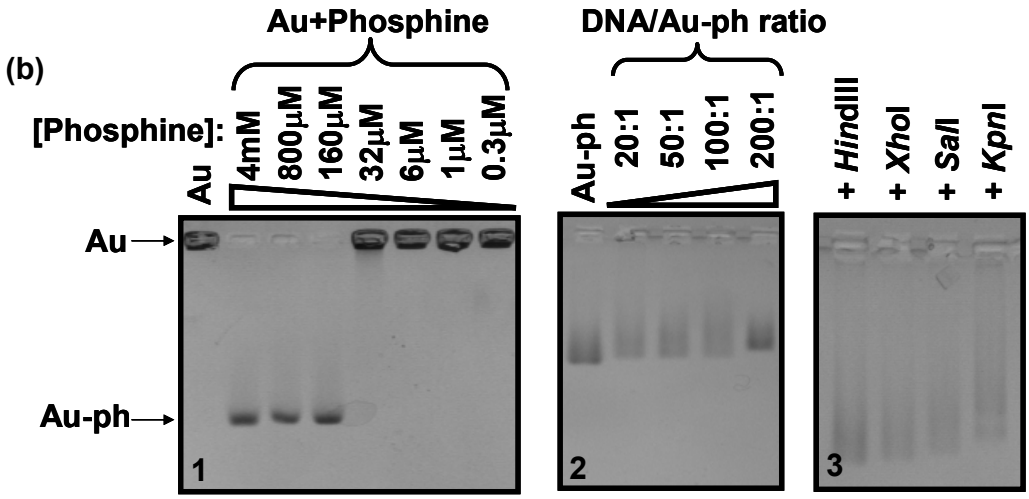
(b)
Au+Phosphine
DNA/Au-ph ratio
[Phosphine]:
Au
4mM
800μM
160μM
32μM
6μM
1μM
0.3μM
Au-ph
20:1
50:1
100:1
200:1
+ HindIII
+ XhoI
+ SalI
+ KpnI
Au
Au-ph
1
2
3

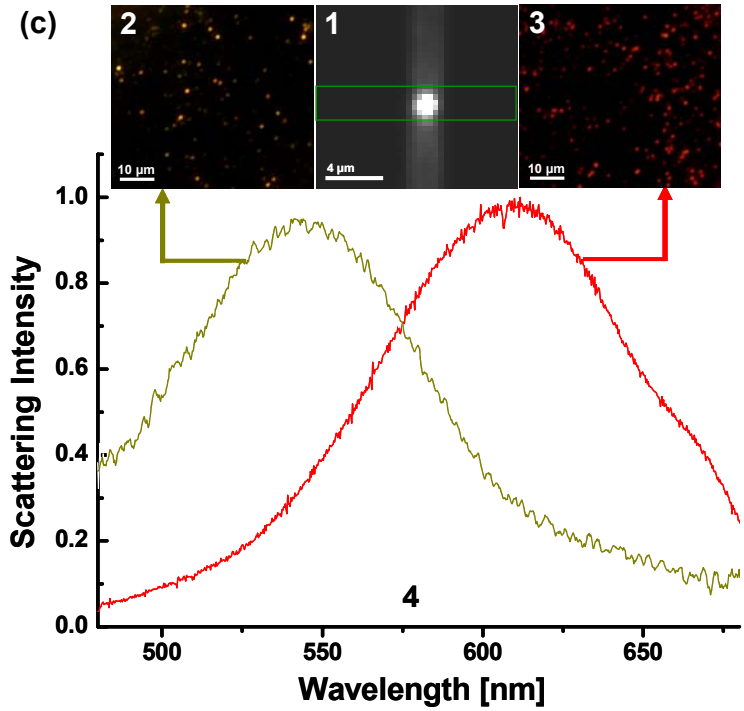
(c)
2
10 μm
1
4 μm
3
10 μm
Scattering Intensity
0.0
0.2
0.4
0.6
0.8
1.0
500
550
600
650
Wavelength [nm]
4

Figure 2

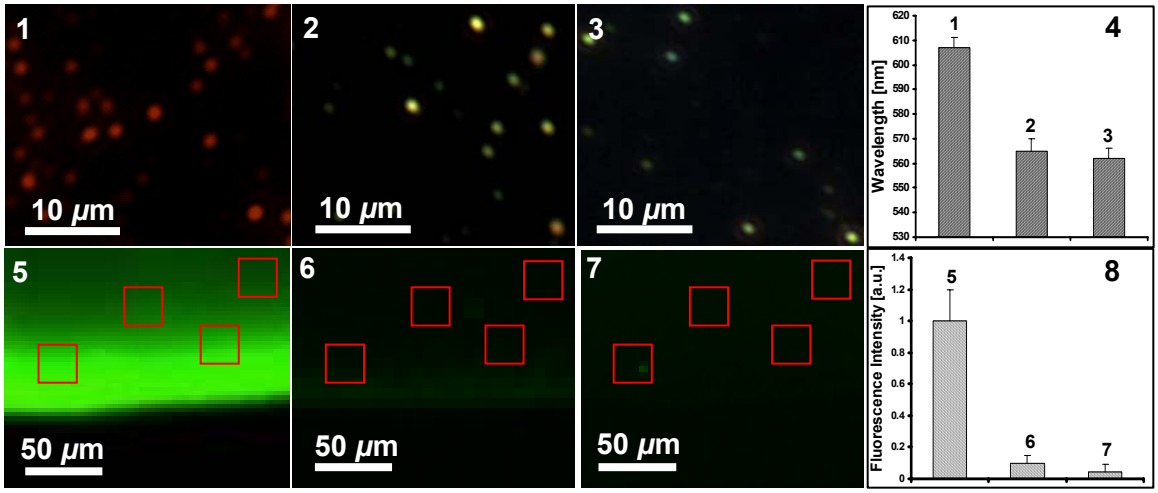
1
2
3
4
10 μm
10 μm
10 μm
Wavelength [nm]
5
6
7
8
50 μm
50 μm
50 μm
Fluorescence Intensity [a.u.]

(a)

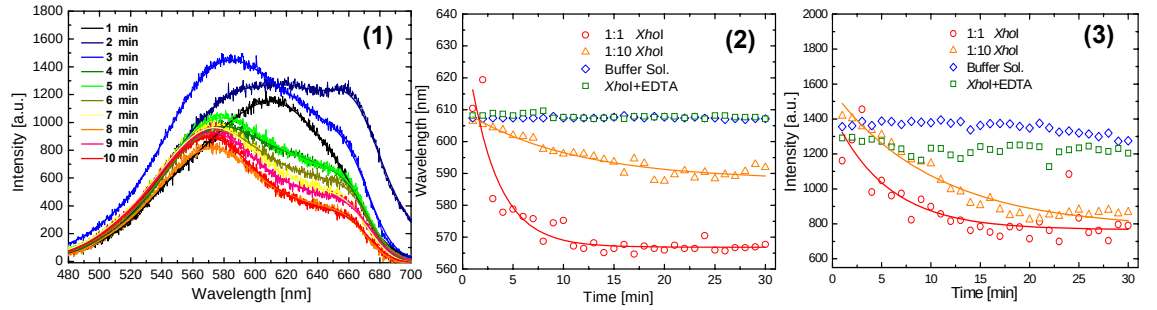
(1)
1 min
2 min
3 min
4 min
5 min
6 min
7 min
8 min
9 min
10 min
Intensity [a.u.]
Wavelength [nm]
(2)
1:1 XhoI
1:10 XhoI
Buffer Sol.
XhoI+EDTA
Wavelength [nm]
Time [min]
(3)
1:1 XhoI
1:10 XhoI
Buffer Sol.
XhoI+EDTA
Intensity [a.u.]
Time [min]

(b)

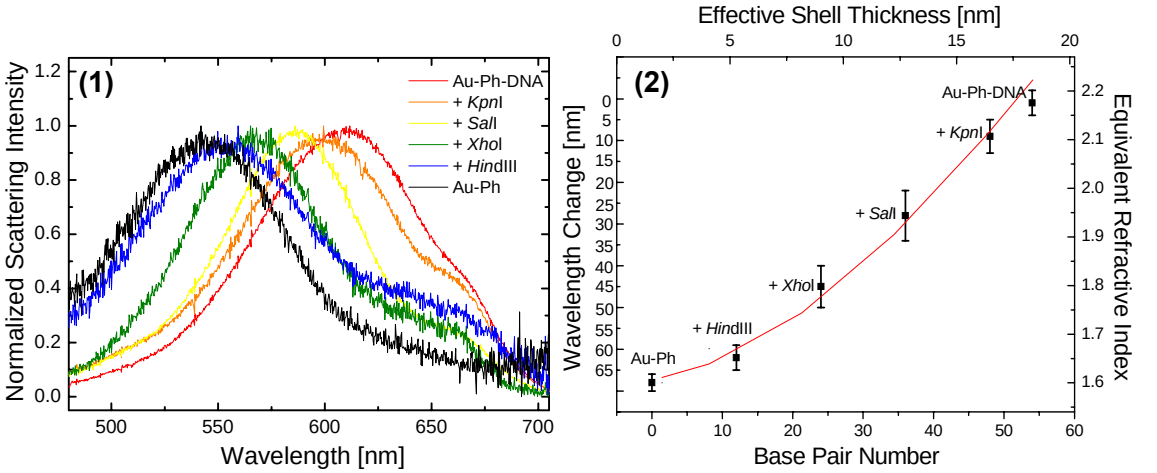
(1)
Au-Ph-DNA
+ KpnI
+ SalI
+ XhoI
+ HindIII
Au-Ph
Normalized Scattering Intensity
Wavelength [nm]
Effective Shell Thickness [nm]
(2)
Au-Ph-DNA
+ KpnI
+ SalI
+ XhoI
+ HindIII
Au-Ph
Wavelength Change [nm]
Equivalent Refractive Index
Base Pair Number

(c)

Figure 3

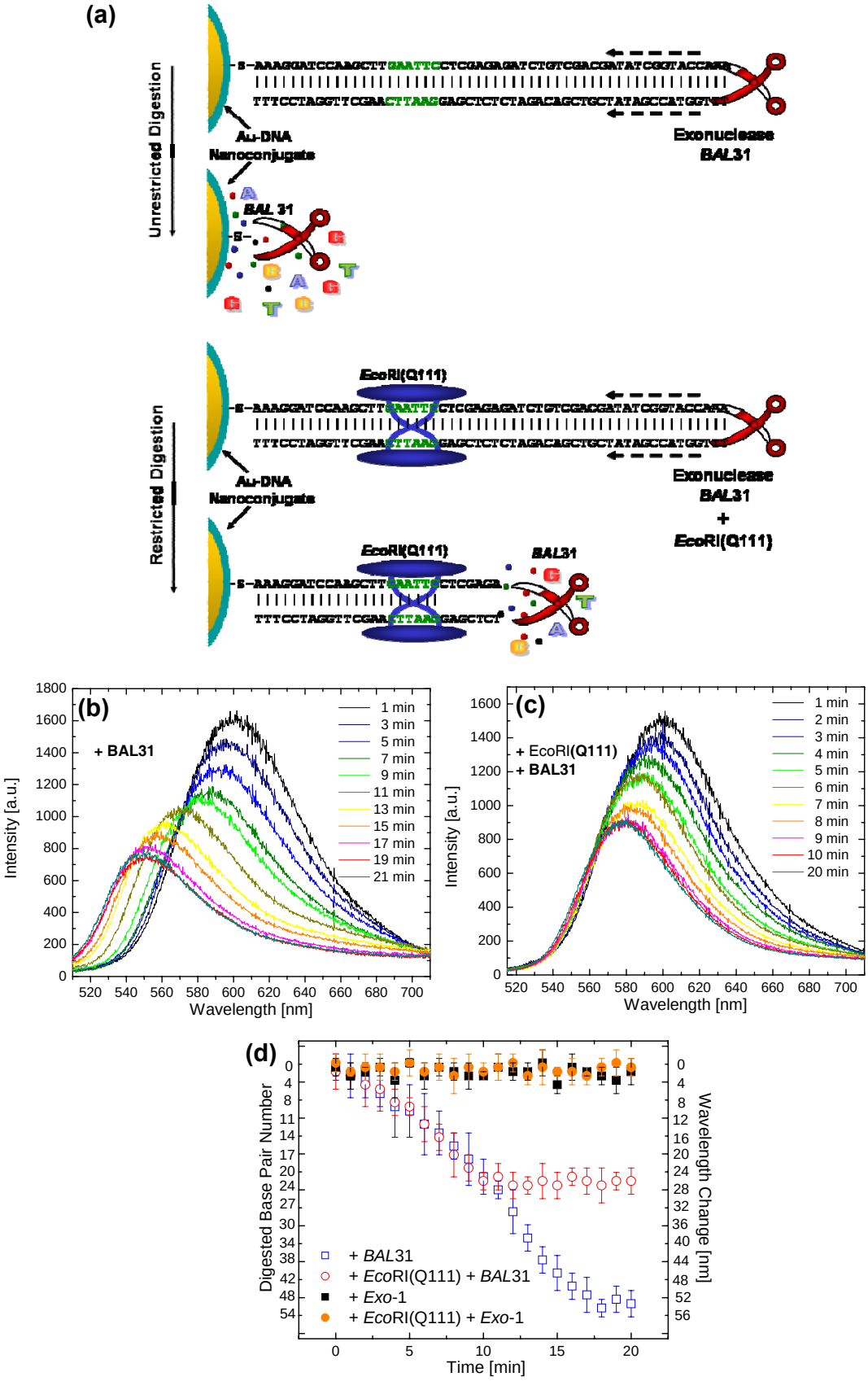
(a)
Unrestricted Digestion
Au-DNA
Nanoconjugate
BAL 31
Exonuclease
BAL31
Restricted Digestion
EcoRI(Q111)
Au-DNA
Nanoconjugate
Exonuclease
BAL31
+
EcoRI(Q111)
EcoRI(Q111)
BAL31
(b)
+ BAL31
1 min
3 min
5 min
7 min
9 min
11 min
13 min
15 min
17 min
19 min
21 min
Intensity [a.u.]
Wavelength [nm]
(c)
+ EcoRI(Q111)
+ BAL31
1 min
2 min
3 min
4 min
5 min
6 min
7 min
8 min
9 min
10 min
20 min
Intensity [a.u.]
Wavelength [nm]
(d)
+ BAL31
+ EcoRI(Q111) + BAL31
+ Exo-1
+ EcoRI(Q111) + Exo-1
Digested Base Pair Number
Wavelength Change [nm]
Time [min]

Figure 4